Chalcogenide Letters Vol. 12, No. 4, April 2015, p. 191 - 201

EFFECT OF LASER ANNEALING ON CdTe THIN FILM DEPOSITED BY THERMAL EVAPORATION

N. A. KHAN[a], K. S. RAHMAN[b], M. I. KAMARUZZAMAN[b], F. HAQUE[a], M. A. ISLAM[a], M. M. ALAM[c], Z. A. ALOTHMAN[c], K. SOPIAN[a], N. AMIN[a,b,c*]
[a]*Solar Energy Research Institute, The National University of Malaysia, 43600 Bangi, Selangor, Malaysia*
[b]*Department of Electrical, Electronic and System Engineering, Faculty of Engineering and Built Environment, The National University of Malaysia, 43600 Bangi, Selangor, Malaysia*
[c]*Advanced Materials Research Chair, Chemistry Department, College of Sciences, King Saud University, Riyadh 11451, Saudi Arabia*

In this study, the influence of laser annealing on the structural, optical and electrical properties of thermally evaporated CdTe thin films has been investigated. CdTe thin films were deposited by thermal evaporation at different power. Thermally evaporated CdTe thin films were then subjected to post deposition laser annealing. The laser annealing was done by illuminating the films by pulsed laser beam with combined wavelengths of 1064nm and 532nm. Both the as-deposited and laser-annealed CdTe thin films were characterized using XRD, AFM, FESEM integrated with EDS, UV-Vis spectroscopy and Hall Effect measurement system. The as-grown and laser-annealed CdTe thin films deposited on soda lime glass showed polycrystalline nature with a mixture of zinc-blende (cubic, C) and wurtzite (hexagonal, H) phases. AFM images on the other hand showed increase in R.M.S roughness value after laser annealing. FESEM micrographs revealed the increase in grain size and the EDS results showed that the CdTe films became tellurium rich upon laser annealing. The band gap of the films increased after laser annealing due to the quantum confinement effect as revealed from optical analysis. Hall Effect measurement found different electrical nature of the CdTe thin films after laser annealing.

(Received March 8, 2015; Accepted April 20, 2015)

Keywords: CdTe thin films, Thermal evaporation, Laser annealing, XRD, FESEM, UV-Vis

1. Introduction

Thin film semiconductors are one of the most promising materials for the fabrication of optoelectronic semiconductor devices. The group II-VI chalcogenides are of the very important series of thin film semiconductors that are well matched for thin film optical devices due to their large optical absorption coefficients and also they can be prepared from inexpensive raw materials by several methods [1-6]. Cadmium telluride (CdTe) is a very attractive and popular photovoltaic material because of its high potential properties which includes high absorption coefficient (5.1×10^5/cm) and ideal energy band gap (Eg) of 1.45eV-1.5eV [6-9]. CdTe has drawn considerable attention in the recent past because of their wide range of use in optoelectronic and photovoltaic applications such as solar cells, infrared and gamma ray detectors, field effect transistors etc [7]. Furthermore, owing to its high absorption coefficient only a thin layer of CdTe of approximately 2μm thickness is required for nearly complete absorption [10]. In thin film heterojunction solar cell fabrication, CdTe can be deposited by various deposition techniques which includes physical

*Corresponding author: nowshad@ukm.edu.my

vapour deposition (PVD) such as close spaced sublimation (CSS), thermal evaporation, RF magnetron sputtering, vapour transport deposition (VTD), metal organic chemical vapour deposition (MOCVD), electro-deposition and screen printing [11-12]. Heterojunction thin film solar cells with multilayer structure require precise annealing process to minimize the inter-diffusion with the layers beneath during the annealing process [13-14]. Laser annealing for thin films has several advantages in comparison to conventional thermal annealing which includes localized high thermal treatments, excellent annealing selectivity to the under layers or substrate, short process duration and precise control of the heating time and zone [15-19].

In this study, CdTe thin films were deposited by thermal evaporation technique which is a physical vapour deposition method (PVD). The films were then subjected to post deposition laser annealing under low vacuum condition. Pulsed Nd:YAG laser system was used to anneal the CdTe thin films at a laser output energy of 60J/pulse and with a combined wavelengths of 1064nm and 532nm. The effect of laser annealing on the structural, optical and electrical properties of CdTe thin films was then investigated.

2. Methodology

CdTe thin films were deposited by thermal evaporation technique on to the commercially available soda lime glasses (SLG) used as substrates. At first the soda lime glasses were cleaned in ultrasonic bath degreased by methanol-acetone-methanol and deionized water for 5 minutes, respectively. Thereafter, N_2 gas was used to dry the degreased glasses. CdTe thin films of thickness approximately 3μm were then deposited on to the ultrasonically cleaned glasses using 99.99% pure CdTe powder by thermal evaporation at various deposition power (measured by current of 26A, 28A and 30A, respectively). The distance between the boat and substrate was kept fixed at 5cm and every time approximately 0.5g of CdTe powder was used during the evaporation. The chamber was evacuated and vacuum condition was maintained during the deposition. When the pressure inside the chamber was significantly low, thermal evaporation was carried out by gradually increasing the current from 0A to the desired value of 26A, 28A and 30A, respectively. The temperature of the boat increased with the increase in current eventually heating the CdTe source and when the temperature reached above the melting point of CdTe, it started to evaporate and the evaporation time was varied in such a way that the thickness of the films were almost uniform for different deposition parameters. After the deposition, the samples were left inside the chamber for natural cooling.

Laser annealing was done on to the thermally evaporated CdTe thin films when the samples had cooled down. The laser annealing was carried out in low vacuum by illuminating with pulsed Nd:YAG laser which has a maximum power output of 1.3 W . The laser beam with output energy of 60J/pulse and a combined wavelength of 1064nm and 532nm were used. The pulse repetition rate was maintained at 10Hz and the scanning velocity for the laser beam irradiance kept constant at 0.5mm/sec. The spot size of 1mm was focused by the Nd:YAG laser system and the working distance of the focusing lens was at 6cm from the substrate.

Table.1: Sample identification with description

Sample I.D.	Sample Description
P1	As-grown at 26A current
P1A2	As-grown at 26A current and laser annealed at 60J/pulse
P2	As-grown at 28A current
P2A2	As-grown at 28A current and laser annealed at 60J/pulse
P3	As-grown at 30A current
P3A2	As-grown at 30A current and laser annealed at 60J/pulse

X-ray diffraction (XRD) was used to analyse the structural properties of CdTe thin films and the surface roughness was measured using atomic force microscopy (AFM). The morphology and the chemical composition of the films were studied by field emission scanning electron microscopy (FESEM) integrated with an energy dispersive X-ray spectrometry (EDS). The optical and the electrical properties were measured from UV-Vis spectrometry and the Hall Effect measurement system, respectively.

3. Results and discussions

3.1 Structural Analysis

XRD analysis was carried out using 'BRUKER aXS-D8 Advance Cu-Kα' diffractometer to analyse the structural properties of CdTe thin films. Quantitative phase analysis of each diffraction pattern was then carried out using the Eva software along with the JCPDS database and the search match tool. The results obtained were then used to analyse the determination of phases, crystallinity, dislocation densities, micro-strain, etc. The XRD pattern in Fig. 1 shows the diffraction peaks for the CdTe thin films which were as-grown at 26A, 28A and 30A and then laser annealed at output energy of 60J/pulse respectively. The XRD pattern for all the samples showed no noticeable peaks except for the polycrystalline CdTe dominating peaks with a mixture of zinc-blende (cubic, C) and wurtzite (hexagonal, H) phases, as shown in Fig. 1 [14,19]. The XRD pattern for all the samples showed two peaks one predominant C(111) at approximately 2θ=23.80 and another small peak C(311) at approximately 2θ =46.50. The XRD pattern obtained are in well agreement with the JCPDS data file (00-015-0770) and (01-073-2871), respectively.

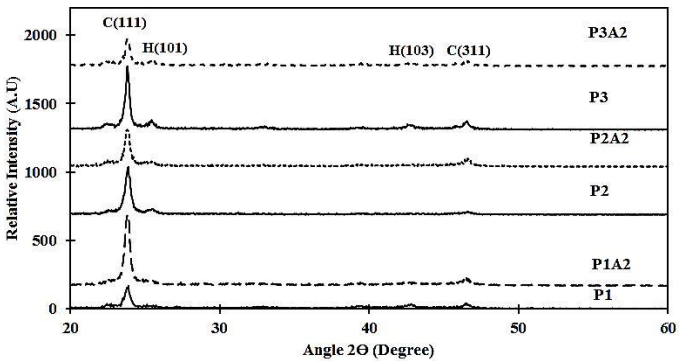

Fig.1: XRD pattern for the as-grown and laser annealed CdTe thin films

Scherrer formula was used to obtain more structural information, the crystallite sizes *D* for the CdTe thin films [20-21].

$$D_{hkl} = 0.9\lambda/(\beta\cos\theta) \quad (1)$$

where, θ is the Bragg diffraction angle, λ is the X-ray wavelength (0.15406 nm) and β is the full width at half maximum [FWHM] of the film diffraction peak at 2θ.

The interspacing between the planes in the atomic lattice, *d* has been calculated using the Brag's Law [22]

$$d_{hkl} = (\lambda/2)\ \mathrm{cosec}\theta \quad (2)$$

where, λ is the X-ray wavelength (0.15406 nm) and θ is the angle between the incident ray and the scattering planes. Lattice misfit is the term which is associated to the micro-strain (ε) developed in the thin films which normally depend on the growth condition. The micro-strain (ε) is calculated from the relation [22-23]

$$\varepsilon = (\beta/4)\tan\theta \quad (3)$$

where, β and θ has their usual significances. The larger value of ε indicates the highly polycrystalline film whereas single crystalline nature exhibits lower micro-strain value. Determining the dislocations density is very important for analysing the crystallographic properties of the thin films.

The dislocation density of thin films was calculated using the Williamson and Smallman's relation [24-25]. In general, dislocations are caused by an imperfection in a crystal which is caused by the miss registry of the lattice in one part of the crystal with respect to another part.

$$\delta = n / D^2 \quad (4)$$

where, n is a factor, which is considered almost equal to unity for minimum dislocation density and 'D' is the crystallite size or grain size.

The above equations were used to calculate the different structural properties which are tabulated in Table.1 below. The crystallite size 'D' along with the other parameters improved for all the films after laser annealing which shows that laser annealing had significant effect on the structural properties of CdTe thin films.

Table.2: Different structural parameters of as-grown and laser annealed CdTe thin films

Samples	**Plane (hkl)**	**d_{hkl} values (nm)**	**Angle 2θ**	**θ (degree)**	**Average D (nm)**	**Micro strain ε ($\times10^{-3}$)**	**Dislocation density δ ($\times10^{11}$ cm^{-2})**
As Grown 26A (P1)	(111) (311)	0.372 0.195	23.88 46.48	0.0036	36.07	1.90	7.67
Laser Annealed 60J/pulse (P1A2)	(111) (311)	0.373 0.195	23.80 46.48	0.0035	40.58	1.84	6.07
As Grown 28A (P2)	(111) (311)	0.372 0.195	23.88 46.62	0.0037	38.65	1.96	6.69
Laser Annealed 60J/pulse (P2A2)	(111) (311)	0.373 0.195	23.80 46.64	0.0036	39.59	1.88	6.38
As Grown 30A (P3)	(111) (311)	0.3734 0.1949	23.80 46.54	0.0029	49.16	1.53	4.14
Laser Annealed 60J/pulse (P3A2)	(111) (311)	0.3731 0.1949	23.80 46.54	0.0030	47.74	1.58	4.38

3.2 Surface Topography Analysis

Atomic force microscope (AFM) was used to measure the surface morphologies of the as-grown and laser annealed CdTe thin films. The figure below shows the 3D surface topography of the CdTe thin films. AFM in general gives microscopic information on the surface structure of the thin films and allows plotting topographies representing the surface relief [25].

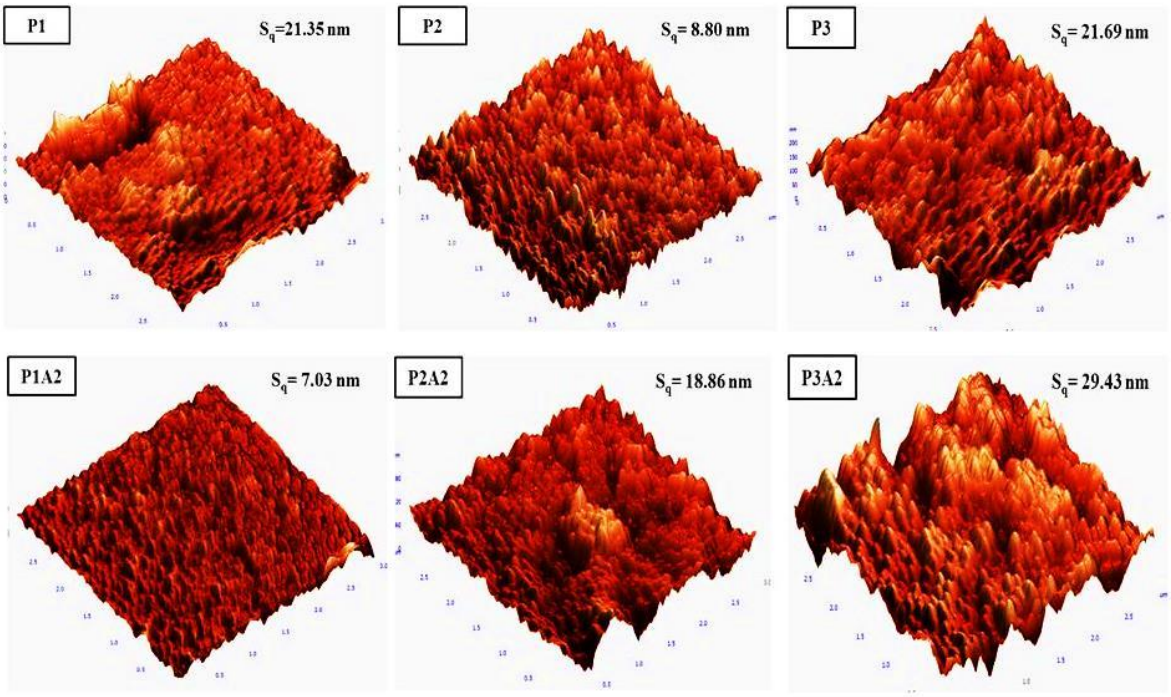

Fig.2: AFM Images of As-grown and Laser Annealed CdTe Thin Films

The root mean square (RMS) roughness 'S_q' of the as-grown and laser annealed CdTe thin films were measured using a NT-MDT atomic force microscope (AFM) and the values was represented graphically. Figure 3 below shows that the roughness value increased slightly after laser annealing for the samples P2A2 and P3A2 which may have attributed towards homogeneous and uniform distribution of CdTe grains throughout the film.

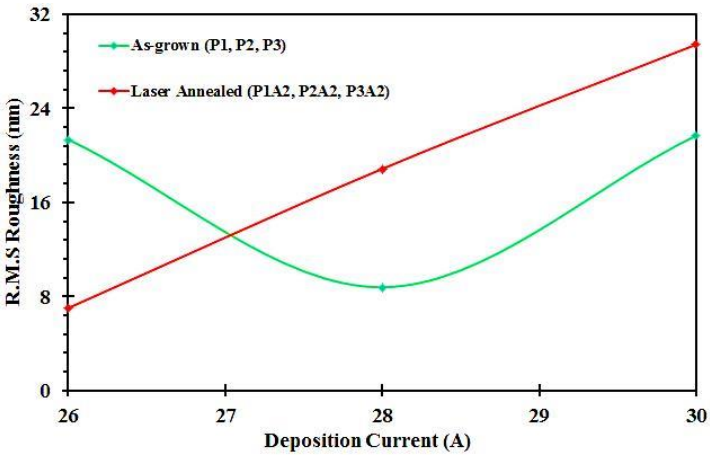

Fig.3: R.M.S Roughness 'Sq' for the as-grown and laser annealed CdTe thin films

3.3 Surface Morphology Analysis

Field emission scanning electron microscopy (FESEM) analysis were performed on the as-grown and laser annealed CdTe thin films to obtain vital surface features of the CdTe thin films.

This analysis provides important information regarding the shape and size of particles or grains and the growth mechanism [26-27]. Figure 5 below shows the images of micrographs obtained for the as-grown and laser annealed CdTe thin films.

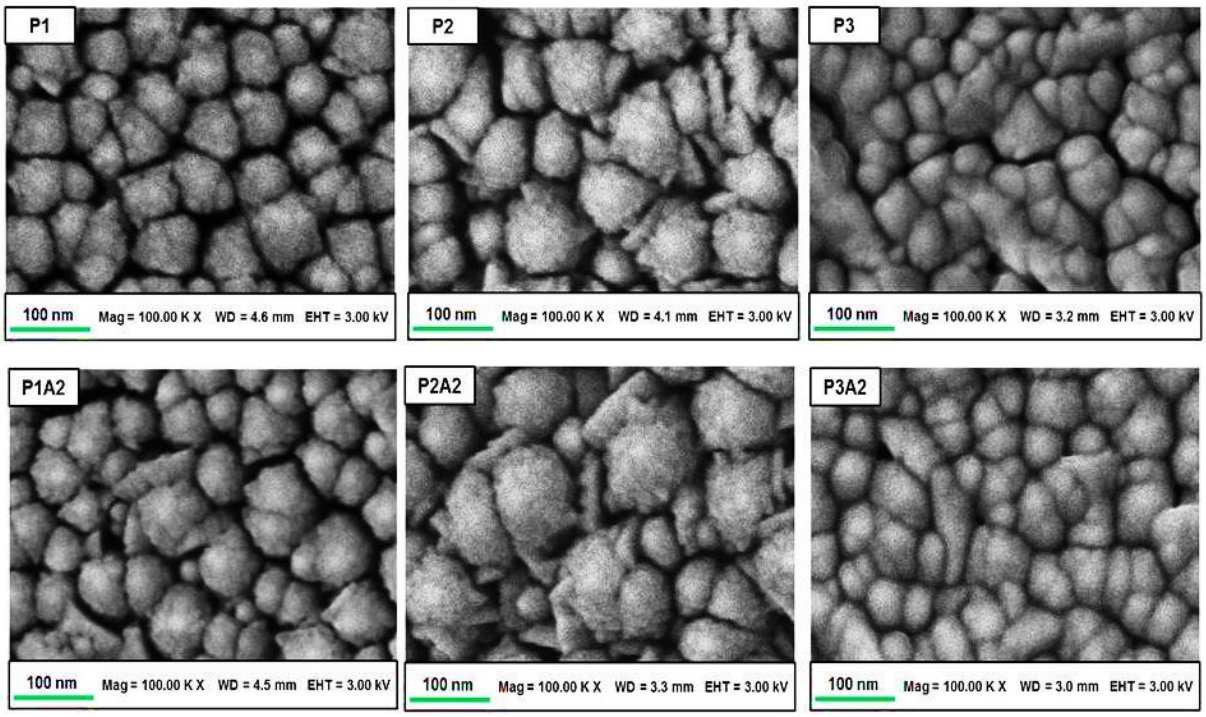

Fig.4: FESEM Images of the as-grown and laser annealed CdTe thin films

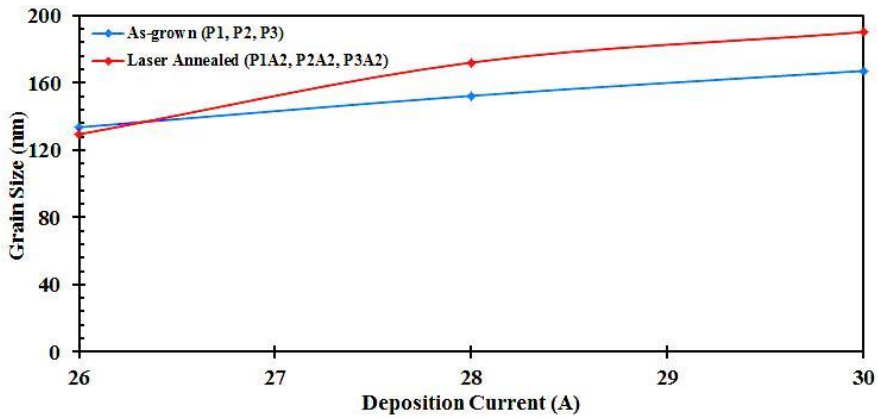

Fig.5: Grain size for the as-grown and laser annealed CdTe thin films

The laser annealing effect could be observed from the above figures. The micrographs in Figure 5 shows that the grain size increased after laser annealing which is also evident from Figure 6 as well. Quantitatively the average grain size for the as-grown and laser annealed films were comparable within a difference of few nanometres. Therefore, the effect of laser annealing on the CdTe thin films were trivial that was observed from the FESEM results.

3.4 Chemical Composition Study

The energy dispersive X-ray spectroscopy (EDS) was generally done to identify different materials present in the samples. The EDS studies were made on the as-grown and laser annealed CdTe thin films to determine the various elements present in the films and their concentration [27-28]. Figure 6 below shows the EDS graph for all the as-grown and laser annealed CdTe thin films.

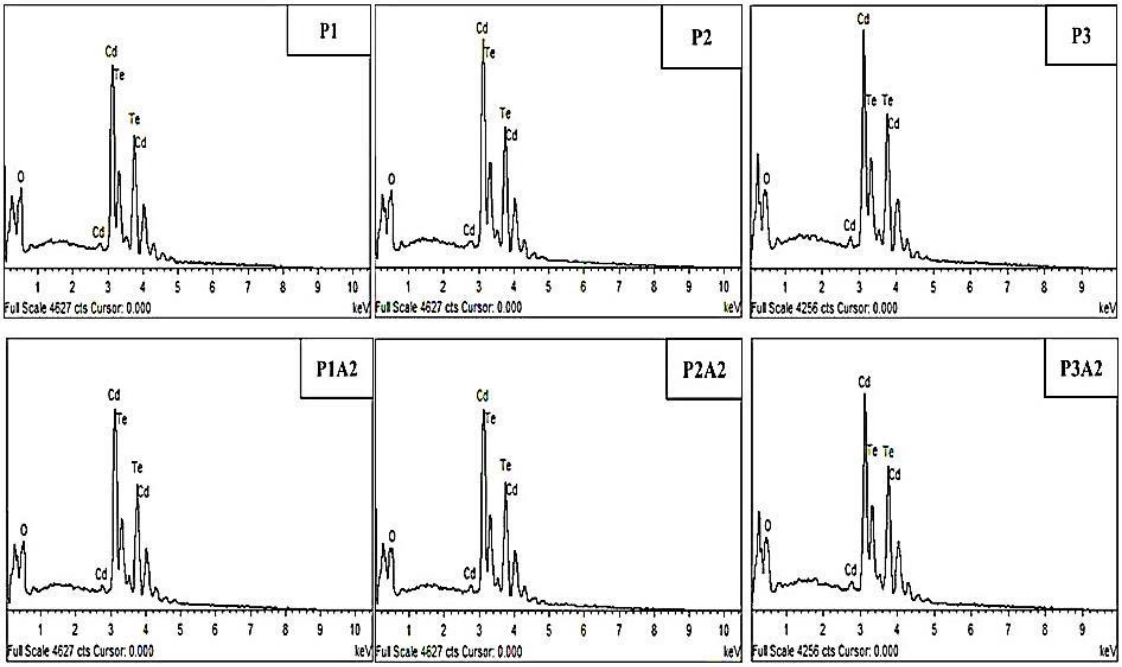

Fig.6: EDS Images of as-grown and laser annealed CdTe thin films

Table.3: Atomic concentration for elements of as-grown and laser annealed CdTe thin films

Samples	Cd (%)	Te (%)	O (%)
As Grown 26A (P1)	40.09	38.98	20.93
Laser Annealed 60 J/pulse (P1A2)	44.41	40.14	15.45
As Grown 28A (P2)	44.75	40.23	15.02
Laser Annealed 60 J/pulse (P2A2)	45.80	41.15	13.04
As Grown 30A (P3)	43.51	40.73	15.76
Laser Annealed 60 J/pulse (P3A2)	43.18	41.82	15.00

The EDS results showed sharp peaks of ‘Cd’ and ‘Te’ together with a small peak of ‘O’ for all the as-grown and laser annealed CdTe thin films. The peaks at 3.1 keV and 3.8 keV depicted the presence of cadmium and tellurium respectively, where as the small peak at 0.5 keV indicated the presence of oxygen. From the atomic concentration table above it shows that all the films became tellurium reach and moreover the oxygen concentration also reduced after the laser annealing was done.

3.5 EDS Mapping

EDS mapping was done on the surface of all the as-grown and laser annealed CdTe thin films in order to check the films quality in more details. Figure 7 below shows the EDS mapping for all the films and from the maps even distribution of ‘Cd’ and ‘Te’ was observed for all the as-grown and laser annealed films. The samples P3 and P3A2 show signs of ‘Te’ rich films which could also be confirmed from Table.3 for atomic concentration.

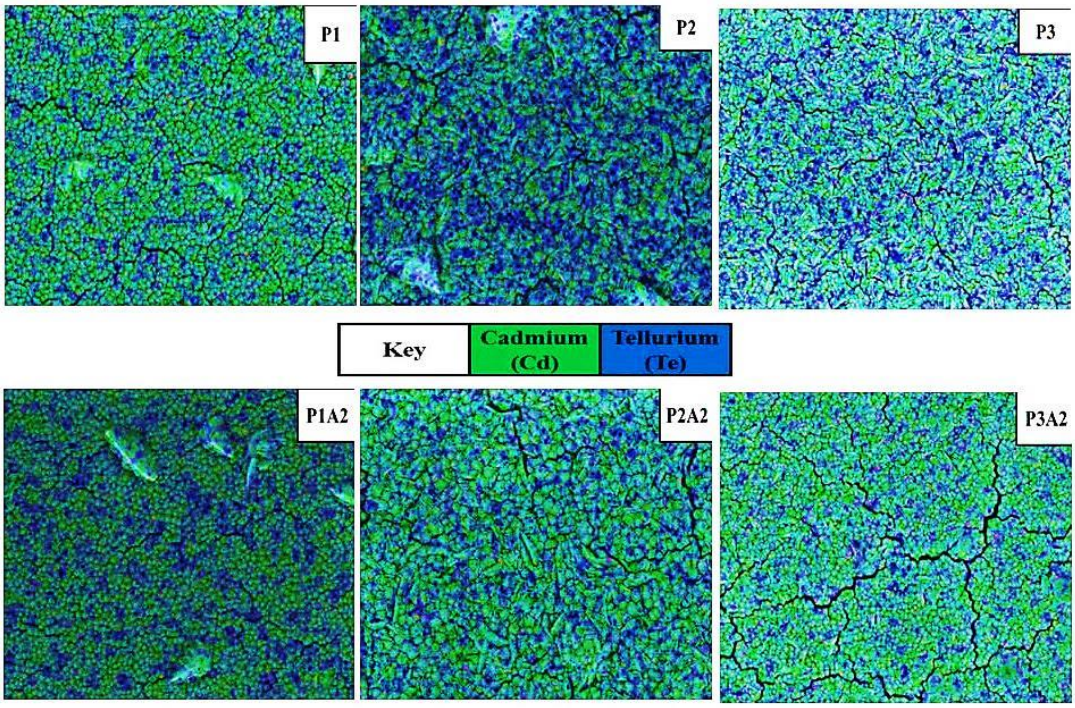

Fig.7: EDS mapping for the as-grown and laser annealed CdTe thin films

3.6 Optical Study

The optical properties of the as-grown and laser annealed CdTe thin films were measured from UV-Vis spectrometry. The transmission spectra and the optical band gap for all the samples were measured. Figure 8 below shows the transmission spectra for all the as-grown and laser annealed films which were carried out between wavelengths of 350 nm to 850 nm. All the films exhibited transmission value below 10% in the visible range which shows that CdTe is a very good absorber layer for solar cells.

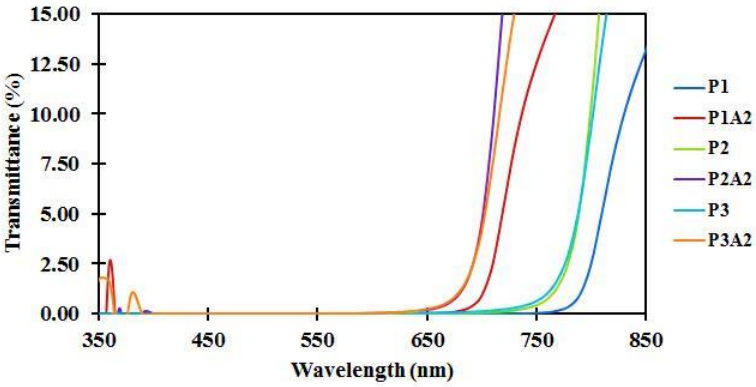

Fig.8: Transmission spectra for the as-grown and laser annealed CdTe thin films

The band gap of the as-grown and laser annealed CdTe thin films were calculated using the following equation which is a well-known expression to calculate the band gap [29].

$$\alpha = A\,(h\eta - Eg)^{1/2} / h\sigma \qquad (5)$$

where, α is the absorption coefficient, A is a constant, hσ is photon energy and Eg is the band gap. The Figure 9 below shows the graph of $(\alpha h\sigma)^2$ against photon energy (hσ), for all the as-grown and laser annealed samples.

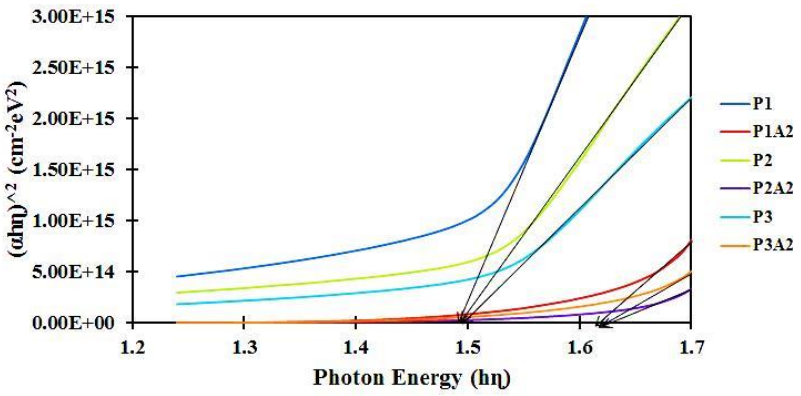

Fig.9: Energy band gap (Eg) for the as-grown and laser annealed CdTe thin films

In comparison to the bulk semiconductors, the increase of the threshold absorption energy in the semiconductor microcrystals is expected to arise from a quantum size effect [30]. The band gap (Eg) increased from 1.5eV to 1.62eV after the laser annealing was done which is due to the quantum confinement effect. The slight shift in band gap could be attributed to the nano-crystallite size depicted from the XRD results and as well as the incorporation of oxygen which could also be confirmed from the EDS table [31-32].

3.7 Electrical Properties Measurement

Electrical properties of the as-grown and laser annealed CdTe thin films were measured using the Hall Effect measurement system. The analysed parameters were bulk concentration, mobility, resistivity and hall coefficient. The system that was used to carry out the measurement was an integrated resistivity/Hall measurement system (ECOPIA 3000). The system had the current source and the magnetic field values constant at 10nA and 0.5T respectively. Table.4 below shows the values of all the parameters obtained from the Hall Effect measurement.

Table.4: Hall Effect measurement data for the as-grown and laser annealed CdTe thin films

Samples	**Bulk Concentration [$\times 10^{12}$] (/cm^3)**	**Mobility (cm^2/Vs)**	**Resistivity [$\times 10^4$] (Ω-cm)**	**Hall Co-efficient [$\times 10^5$] (cm^3/C)**
As Grown 26A (P1)	4.22	27.77	7.67	21.36
Laser Annealed 60 J/pulse (P1A2)	2.26	39.75	7.19	28.35
As Grown 28A (P2)	8.73	31.79	3.20	6.83
Laser Annealed 60 J/pulse (P2A2)	1.73	62.53	6.66	42.39
As Grown 30A (P3)	3.25	83.75	8.04	72.95
Laser Annealed 60 J/pulse (P3A2)	6.39	35.55	8.61	10.24

To observe the relation between bulk concentration and resistivity for the as-grown and laser annealed CdTe thin films, two graphs in Figure 10 were plotted. For the first figure the

variation of bulk concentration with resistivity for the as-grown samples were shown which revealed a straight forward nature that with the increase in bulk concentration, the resistivity of the films decreases. On the other hand similar nature was not observed for the laser annealed films in Figure 10 (b) where the resistivity didn't reduce with the increase in bulk concentration because for the laser annealed films, the mobility increased upon laser annealing which intern causes hindrance for the movement of charge carriers eventually increasing the resistivity of the films.

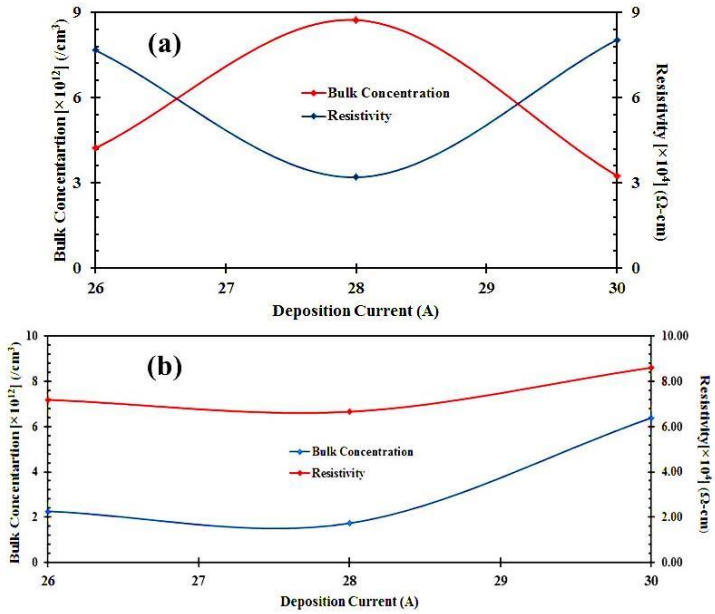

Fig. 10: (a) As-grown CdTe films (b) Laser annealed CdTe films

4. Conclusion

In this study, the effects of laser annealing on the thermally evaporated CdTe thin films were observed. The conclusions are made based on the structural, optical and electrical analysis which was carried out in this study. XRD results showed that the films were polycrystalline in nature with a mixture of zinc-blende (cubic, C) and wurtzite (hexagonal, H) phases. AFM revealed that the R.M.S roughness increases after laser annealing. The chemical analysis showed that the films become tellurium rich after laser annealing which is desirable. The optical measurement depicted that the band gap of the samples increases after laser annealing possibly due to quantum confinement effect. Electrical properties showed that the mobility increases after laser annealing which in turn increases the film resistivity. The above results illustrated that laser annealing has some significant effect on certain properties of CdTe thin films suitable for PV application.

Acknowledgement

The authors would like to acknowledge and appreciate the contribution of the Ministry of Education of Malaysia through its research grants with code FRGS/1/2014/TK06/UKM/01/1 and DIP-2014-010. Appreciations are also extended to the VP unit of the King Saud University (KSU) of Saudi Arabia.

References

[1] H. Hernandez-Contreras, G. Contreras-Puente, J. Aguilar-Hernandez, A. Morales-Acevedo, J. Vidal-Larramendi, O. Vigil-Galan, Thin Solid Films **403-404,** 148 (2002).
[2] A.U. Ubale, R.J. Dhokne, P.S. Chikhlikar, V.S. Sangawar, D.K. Kulkarni, Bull Mater Sci

29, 165 (2006).
[3] S. Tewari, A. Bhattacharjee, P. P. Sahay, J Mater Sci **44**, 534 (2009).
[4] T.L. Chu, S.S. Chu, Prog Photovolt **1**, 31 (1993).
[5] M. Godlewski and A. Zakrzewski, "Nonradiative recombination processes in II-VI luminophors", chapter in II-VI Semiconductor Compounds, ed. M. Jain, World Scientific,Singapore, 205 (1993).
[6] M.A Islam, Q Huda, M.S Hossain, M.M Aliyu, M.R Karim, K.Sopian, N.Amin, Current Applied Physics **13**, 115 (2013).
[7] R.H. Williams, M.H. Patterson, Applied Physics Letters **40**, 484 (1982).
[8] S. Lalitha, R. Sathyamoorthy, S. Senthilarasu, A. Subbarayan, K. Natarajan, Solar Energy Materials & Solar Cells **82**, 187 (2004).
[9] H. Uda, S. Ikegami, H. Sonomura, Jpn. J. Appl. Phys. **29**, 2003 (1990).
[10] A. Abbas, G. D. West, J. W. Bowers, P. Isherwood, P. M. Kaminski, B. Maniscalco, P. Rowley, J. M. Walls, K. Barricklow, W. S. Sampath, K. L. Barth, IEEE Journal of Photovoltaics **3**, 1361 (2013).
[11] Brian E. McCandless and James R. Sites, Handbook of Photovoltaic Science and Engineering, John Wiley & Sons Ltd (2003).
[12] N. A. Khan, K. S. Rahman, F. Haque, N. Dhar, M. A. Islam, M. Akhtaruzzaman, K. Sopian, N. Amin, presented at the 8th International Conference on Electrical and Computer Engineering (ICECE 2014), December 20-22 -nd , 2014, Dhaka Bangladesh.
[13] A. Matsuno, E. Takii, T. Eto, K. Kurobe and K. Shibahara, Phys. Res. B **237**, 136 (2005).
[14] N. H. Kim, C. I. Park and J. Park, J. Korean Phys. Soc. **62**, 502 (2013).
[15] D. Sands, J. E. Nicholls, J. H. C. Hogg, S. Chalk, F. X. Wagner, W. E. Hagstona, M. O'Neill, B. Lunn, D. E. Ashenford, J. Cryst. Growth **184/185**, 114 (1998).
[16] W. Tang, Z. Chen, S. He and H. Zhang, Procedia Chem. **1**, 786 (2009).
[17] L. Schade, S. Franzka, S. Hardt, H. Wiggers and N. Hartmann, Appl. Surf. Sci. **278**, 336 (2013).
[18] M. G. Kang, K. H. Cho, S. M. Oh, Y. H. Do, C. Y. Kang, S. Kim and S. J. Yoon, Curr. Appl. Phys. **11**, 66 (2011).
[19] N. Kim and C. II. Park, Journal of the Korean Physical Society, **63**, 229 (2013).
[20] B. E. Warren, X-ray Diffraction, Dover publications, (1990).
[21] K. Sarmah, R. Sarma, H. L. Das, Chalcogenide Letters, **5**(8), 153 (2008).
[22] M.A. Islam, M.S. Hossain, M.M. Aliyu, M.R. Karim, T. Razykov, K. Sopian, N. Amin, Thin Solid Films, Thin Solid Films, **546**, 367 (2013).
[23] K.S. Rahman, F. Haque, N.A. Khan, M. A. Islam, M.M. Alam, Z.A. Alothman, K. Sopian, N. Amin, Chalcogenide Letters, **11**, 129 (2014).
[24] M. Dhanam, B. Kavitha, Neetha Jose, Dheera P Devasia, Chalcogenide Letters, **6**(12), 713 (2009).
[25] M. A. Islam, M. H. Hossain, M.M. Aliyu, Y. Sulaiman, M.R. Karim, K. Sopian, N. Amin, presented at 7th International Conference on Electrical and Computer Engineering (ICECE-2012), December 20-22 nd, 2012, Dhaka, Bangladesh.
[26] S.D. Chavhan, S. Senthilarasu, Soo-Hyoung Lee, Applied Surface Science **254**, 4539 (2008).
[27] T. Hryniewicz, K. Rokosz, H.R. Zschommler Sandim, Applied Surface Science **263**, 357 (2012).
[28] A.L. Dawar, C. Jagadish, K.V. Ferdinand, A. Kumar, P.C. Mathur, Applications of Surface Science **22/23**, 846 (1985).
[29] J C Osuwa, C I Oriakuand I. A. KALU, Chalcogenide Letters, **6,** 433 (2009).
[30] H. Arizpe-Chavez, R. Ramırez-Bon, F.J. Espinoza-Beltran, O. Zelaya-Angel, J.L. Marın, R. Riera, Journal of Physics and Chemistry of Solids **61**, 511 (2000).
[31] S.K. Pandeya, Umesh Tiwari, R. Raman, Chandra Prakash, Vamsi Krishna, Viresh Dutta, K. Zimik, Thin Solid Films **473**, 54 (2005).
[32] H. Arizpe-Chavez, F. J. Espinoza-Beltran, R. Ramirez-Bon, O. Zelaya-Angel, J. Gonzalez-Hernandez, Solid State Communications **101**, 39 (1997).